A new broad-band spectral state in the ultraluminous X-ray source Holmberg IX X-1

D. J. Walton [iD],[1]* M. Bachetti [iD],[2] P. Kosec,[3] F. Fürst,[4] C. Pinto,[5] T. P. Roberts [iD],[6] R. Soria [iD],[7,8] D. Stern,[9] W. N. Alston [iD],[1] M. Brightman,[10] H. P. Earnshaw [iD],[10] A. C. Fabian [iD],[11] F. A. Harrison,[10] M. J. Middleton[12] and R. Sathyaprakash[13]

[1]*Centre for Astrophysics Research, University of Hertfordshire, College Lane, Hatfield AL10 9AB, UK*
[2]*INAF – Osservatorio Astronomico di Cagliari, via della Scienza 5, I-09047 Selargius, Italy*
[3]*Center for Astrophysics – Harvard, Smithsonian, Cambridge, MA 02138, USA*
[4]*European Space Astronomy Centre (ESA/ESAC), Operations Department, Villanueva de la Cañada, 28692 Madrid, Spain*
[5]*INAF – IASF Palermo, Via U. La Malfa 153, I-90146 Palermo, Italy*
[6]*Centre for Extragalactic Astronomy and Department of Physics, Durham University, South Road, Durham DH1 3LE, UK*
[7]*INAF – Osservatorio Astrofisico di Torino, Strada Osservatorio 20, I-10025 Pino Torinese, Italy*
[8]*Sydney Institute for Astronomy, School of Physics A28, The University of Sydney, Sydney NSW 2006, Australia*
[9]*Jet Propulsion Laboratory, California Institute of Technology, Pasadena, CA 91109, USA*
[10]*Cahill Center for Astronomy and Astrophysics, California Institute of Technology, 1200 E. California Boulevard, Pasadena, CA 91125, USA*
[11]*Institute of Astronomy, University of Cambridge, Madingley Road, Cambridge CB3 0HA, UK*
[12]*Department of Physics and Astronomy, University of Southampton, Highfield, Southampton SO17 1BJ, UK*
[13]*Astronomia e astrofisica, Scuola Universitaria Superiore IUSS Pavia, Palazzo del Broletto, Piazza della Vittoria 15, I-27100 Pavia, Italy*

ABSTRACT

We present a series of five new broad-band X-ray observations of the ultraluminous X-ray source Holmberg IX X-1, performed by *XMM–Newton* and *NuSTAR* in coordination. The first three of these show high-soft X-ray fluxes but a near total collapse of the high-energy ($\gtrsim 15$ keV) emission, previously seen to be surprisingly stable across all prior broad-band observations of the source. The latter two show a recovery in hard X-rays, remarkably once again respecting the same stable high-energy flux exhibited by all of the archival observations. We also present a joint analysis of all broad-band observations of Holmberg IX X-1 to date (encompassing 11 epochs in total) in order to investigate whether it shows the same luminosity–temperature behaviour as NGC 1313 X-1 (which also shows a stable high-energy flux), whereby the hotter disc component in the spectrum exhibits two distinct, positively-correlated tracks in the luminosity–temperature plane. Holmberg IX X-1 may show similar behaviour, but the results depend on whether the highest energy emission is assumed to be an up-scattering corona or an accretion column. The strongest evidence for this behaviour is found in the former case, while in the latter the new 'soft' epochs appear distinct from the other high-flux epochs. We discuss possible explanations for these new 'soft' spectra in the context of the expected structure of super-Eddington accretion flows around black holes and neutron stars, and highlight a potentially interesting analogy with the recent destruction and re-creation of the corona seen in the AGN 1ES 1927 + 654.

Key words: X-rays: binaries – X-rays: individual (Holmberg IX X-1).

1 INTRODUCTION

The *NuSTAR* era has brought about significant progress in our understanding of the ultraluminous X-ray source (ULX) population. Seen almost exclusively in other galaxies, these are the most extreme members of the X-ray binary population and exhibit luminosities in excess of 10^{39} erg s^{-1} (the Eddington limit for a typical ~ 10 M$_\odot$ stellar remnant black hole); see A. King, J.-P. Lasota & M. Middleton (2023) and C. Pinto & D. J. Walton (2023) for recent reviews. Explanations for these extreme luminosities in the literature typically

focused on either sub-Eddington accretion on to intermediate mass black holes (IMBHs, $M_{BH} \sim 10^{2-5}$ M$_\odot$; e.g. J. M. Miller et al. 2003; T. E. Strohmayer & R. F. Mushotzky 2009) or super-Eddington accretion on to relatively normal stellar remnants (e.g. A. R. King et al. 2001; J. Poutanen et al. 2007). However, we now understand the majority of ULXs to represent the best local examples of the latter. *NuSTAR* (F. A. Harrison et al. 2013) has enabled detailed studies of ULXs in the hard X-ray band ($E \gtrsim 10$ keV) for the first time, revealing broad-band spectra inconsistent with standard modes of sub-Eddington accretion (e.g. M. Bachetti et al. 2013; D. J. Walton et al. 2013a, 2015a, b; E. S. Mukherjee et al. 2015; V. Rana et al. 2015; H. P. Earnshaw et al. 2019; M. Brightman et al. 2022), confirming prior indications seen at lower energies (e.g. A.-M. Stobbart, T. P.

*E-mail: d.walton4@herts.ac.uk

Roberts & J. Wilms 2006; J. C. Gladstone, T. P. Roberts & C. Done 2009). More importantly, *NuSTAR* observations of the M82 galaxy resulted in the discovery of the first ULX pulsar (M. Bachetti et al. 2014), unambiguously identifying the accretor as a highly super-Eddington neutron star. Since this discovery, at least five more ULX pulsars have been revealed (F. Fürst et al. 2016; G. L. Israel et al. 2017b, a; S. Carpano et al. 2018; R. Sathyaprakash et al. 2019; G. A. Rodríguez Castillo et al. 2020; F. Pintore et al. 2025). High-resolution spectroscopy with *XMM–Newton* (J. W. den Herder et al. 2001; F. Jansen et al. 2001) has also recently revealed the presence of powerful outflows in a number of ULXs (C. Pinto, M. J. Middleton & A. C. Fabian 2016; D. J. Walton et al. 2016a; C. Pinto et al. 2017, 2020; P. Kosec et al. 2018a, b, 2021), further cementing the association between ULXs and super-Eddington accretion as such winds are a ubiquitous prediction for this regime.

Holmberg IX X-1 is one of the better studied members of the ULX population, although as no X-ray pulsations have ever been seen from this source (V. Doroshenko, A. Santangelo & L. Ducci 2015, D. J. Walton et al. 2017a; Appendix A) the nature of the accretor remains unknown. Located at a distance of 3.55 Mpc (G. Paturel et al. 2002), it is one of the nearest ULXs that almost persistently exhibits luminosities in excess of 10^{40} erg s^{-1}. Studies of Holmberg IX X-1 have generally mirrored the same evolution as studies of the broader ULX population. Early observations with *XMM–Newton* revealed potential evidence for a low-temperature accretion disc ($kT \sim 0.2$–0.3 keV, consistent with the idea that this may host a $\sim 1000\,M_\odot$ IMBH J. M. Miller et al. 2003). However, higher signal-to-noise (S/N) data subsequently showed evidence that the emission in the 2–10 keV band was not a standard sub-Eddington power-law continuum (e.g. J. C. Gladstone et al. 2009; D. J. Walton et al. 2013b), which was further confirmed by high-energy observations with *INTEGRAL* (S. Y. Sazonov, A. A. Lutovinov & R. A. Krivonos 2014) and with coordinated broad-band observations combining *XMM–Newton*, *Suzaku* (K. Mitsuda et al. 2007), and *NuSTAR* (D. J. Walton et al. 2014; see also W. Luangtip, T. P. Roberts & C. Done 2016). Further broad-band follow-up combining *Suzaku* and *NuSTAR* showed unusual spectral variability: strong variations were seen between observing epochs at lower energies ($\lesssim 10$ keV), with the peak of the X-ray spectrum shifting to lower energies at higher fluxes, while the high-energy flux ($\gtrsim 15$ keV) remained comparatively stable (D. J. Walton et al. 2017a; see also A. Gúrpide et al. 2021). Similar behaviour has also been seen in multi-epoch broad-band observations of another well-studied ULX, NGC 1313 X-1 (D. J. Walton et al. 2020), but its origin is not currently well understood.

With the availability of broad-band data for ULXs in the *NuSTAR* era, standard spectral models for these sources have come to include two thermal accretion disc components (typical temperatures ~ 0.2–0.5 and ~ 1–3 keV; e.g. D. J. Walton et al. 2014, 2018c; F. Koliopanos et al. 2017) – the cooler of which may be associated with a combination of emission from the outer disc and the large wind expected for super-Eddington accretion, while the hotter may be associated with the innermost, funnel-like regions of a super-Eddington disc – and an additional steep high-energy continuum component (either from an accretion column or an up-scattering corona; e.g. E. S. Mukherjee et al. 2015; D. J. Walton et al. 2015a, 2018c). When the multi-epoch data for NGC 1313 X-1 were fit with these models (the nature of the accretor in NGC 1313 X-1 is also not yet known) the evolution of the hotter disc component exhibited some unusual behaviour in the luminosity–temperature plane. The broad-band observations showed two distinct groups, consisting of a set with lower fluxes and higher temperatures, and a set with higher fluxes but lower temperatures. However, both of these individual

groups showed evidence for having its own *positive* luminosity–temperature relation (i.e. higher temperatures at higher fluxes), such that the inner disc component appeared to be following two distinct luminosity–temperature tracks. This strange luminosity–temperature behaviour is itself challenging to understand, but also made it even more difficult to understand the relative consistency of the highest energy data.

While the nature of this spectral evolution is still not clear, it is important to establish whether the same behaviour is seen in other sources. As noted above, the same kind of evolution appears to be present in Holmberg IX X-1, but the archival data only include one observation that would correspond to the high-flux, low-temperature group seen in NGC 1313 X-1.

Here, we present a set of five new broad-band observations of Holmberg IX X-1 with *XMM–Newton* and *NuSTAR* that allow us to further explore the strange spectral variability seen from this source. The main result from these new observations is the revelation of a new, soft broad-band spectral 'state' – seen during the first three of these new observations – in which the previously stable high-energy flux has collapsed (though the source does subsequently recover to the same high-energy flux in the latter two). The rest of the paper is structured as follows: the new observations and our data reduction are described in Section 2, and our spectral analysis is presented in Section 3. The results from this analysis are discussed in Section 4 (including a detailed consideration of the potential nature of this new soft state in Section 4.2), a brief exploration into the advances that a mission similar to the recently-proposed *High Energy X-ray Probe* (*HEX-P*; K. K. Madsen et al. 2024) would provide for broad-band studies of ULXs is presented in Section 5, and finally our main conclusions are summarized in Section 6.

2 OBSERVATIONS AND DATA REDUCTION

During the course of late 2020 (October–November), *XMM–Newton* and *NuSTAR* performed a series of five new coordinated observations of Holmberg IX X-1.[1] In total, there are now 11 epochs of coordinated broad-band X-ray observations of Holmberg IX X-1 taken with some combination of *NuSTAR*, *XMM–Newton*, and *Suzaku*. These new observations (broad-band epochs 7–11) were triggered on the transition to a high-flux state below 10 keV, detected by monitoring with the *Neil Gehrels Swift Observatory* (hereafter *Swift*; N. Gehrels et al. 2004); we show them in the context of the long-term evolution of Holmberg IX X-1 seen by the *Swift* XRT (D. N. Burrows et al. 2005) in Fig. 1. The following sections describe these new observations in more detail, and outline our data reduction procedure. Basic information for all the broad-band observations considered in this work is given in Table 1.

2.1 *NuSTAR*

We reduced the *NuSTAR* data following standard procedures with the *NuSTAR* Data Analysis Software (v2.0.0; part of the HEASOFT distribution) and *NuSTAR* caldb v20211202. The raw event files for each observation were initially cleaned with NUPIPELINE, using the

---

[1]Four new observations were originally planned, but during the third *XMM–Newton* exposure (OBSID 0870930401) the EPIC-MOS detectors experienced a fault, and so a fifth observation was scheduled. However, the EPIC-pn detector was still fully operational during this third observation, and the EPIC-MOS detectors did operate for the last ~ 25–30 per cent of the exposure, so we still analyse the data that is available for this observation.
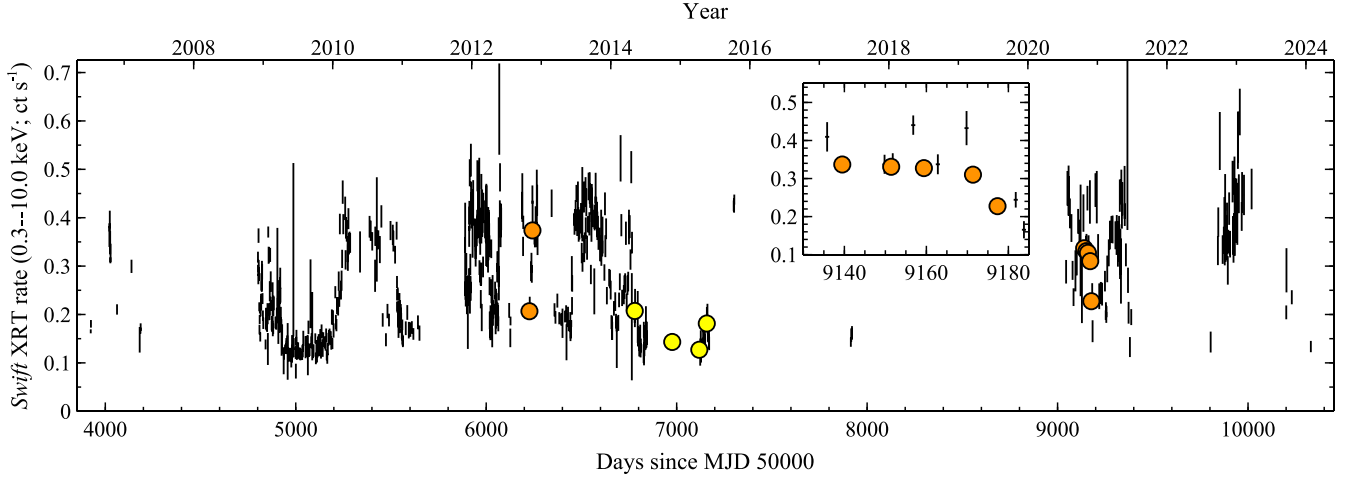
Figure 1. The long-term X-ray lightcurve of Holmberg IX X-1 seen by *Swift*/XRT (1d time bins), extracted using the online pipeline (P. A. Evans et al. 2009). The broad-band observations considered here are shown with the large orange/yellow circles, after converting the *XMM–Newton/Suzaku* data to equivalent XRT count rates based on their observed spectra. The inset shows a zoom-in on the most recent series of broad-band observations.

Table 1. Details of the broad-band observations of Holmberg IX X-1 used in this work (given in chronological order).

Epoch	Mission(s)	OBSID(s)	Start date	Exposure[a] (ks)
1	*Suzaku*	707019020	2012-10-21	107
	XMM–Newton	0693850801	2012-10-23	10/14
	Suzaku	707019030	2012-10-24	107
	XMM–Newton	0693850901	2012-10-25	11/14
	Suzaku	707019040	2012-10-26	110
	NuSTAR	30002033002	2012-10-26	43
	NuSTAR	30002033003	2012-10-26	124
	XMM–Newton	0693851001	2012-10-27	11/13
2	*NuSTAR*	30002033005	2012-11-11	49
	NuSTAR	30002033006	2012-11-11	41
	XMM–Newton	0693851701	2012-11-12	7/10
	NuSTAR	30002033008	2012-11-14	18
	XMM–Newton	0693851801	2012-11-14	10//9
	NuSTAR	30002033010	2012-11-15	59
	XMM–Newton	0693851101	2012-11-16	10/13
3	*NuSTAR*	30002034002	2014-05-02	81
	Suzaku	707019010	2014-05-03	32
4	*NuSTAR*	30002034004	2014-11-15	81
	Suzaku	707019020	2014-11-15	34
5	*NuSTAR*	30002034006	2015-04-06	64
	Suzaku	707019030	2015-04-06	32
6	*NuSTAR*	30002034008	2015-05-16	67
	Suzaku	707019040	2015-05-16	34
7	*NuSTAR*	80602308002	2020-10-17	66
	XMM–Newton	0870930101	2020-10-17	16/22
8	*NuSTAR*	80602308004	2020-10-29	66
	XMM–Newton	0870930301	2020-10-29	16/14
9	*NuSTAR*	80602308006	2020-11-05	76
	XMM–Newton	0870930401	2020-11-06	17/7[b]
10	*NuSTAR*	80602308008	2020-11-18	64
	XMM–Newton	0870930501	2020-11-18	18/25
11	*NuSTAR*	80602308010	2020-11-23	69
	XMM–Newton	0870931001	2020-11-24	17/24

[a]*XMM–Newton* exposures are listed separately for the EPIC-pn/MOS detectors after background filtering, and the *NuSTAR* exposures combine both modes 1 and 6; all exposures are given to the nearest ks.
[b]The EPIC-MOS detectors experienced a fault during this observation, hence the reduced exposure.

standard depth correction to reduce the internal background. Passages through the South Atlantic Anomaly and periods during which Holmberg IX X-1 was occulted by the earth were also excluded. Source products were extracted from the cleaned event files for each focal plane module (FPMA, FPMB) using NUPRODUCTS. We used circular regions of radius ∼ 75 arcsec for the source aperture, and the background was estimated from a larger, blank area on the same detector, free of contaminating point sources. In addition to the standard 'science' data (mode 1), we also extract the 'spacecraft science' data (mode 6) in order to maximize the signal-to-noise (S/N), following D. J. Walton et al. (2016b). This provides ∼20–40 per cent of the total good exposure, depending on the specific observation.

2.2 *XMM–Newton*

The *XMM–Newton* observations were also reduced following standard procedures with the *XMM–Newton* Science Analysis System (v19.1.0). For the EPIC-pn and EPIC-MOS CCD detectors (L. Strüder et al. 2001; M. J. L. Turner et al. 2001) we processed the raw data files for each observation using EPCHAIN and EMCHAIN to produce calibrated event lists. For these new *XMM–Newton* exposures, each of the EPIC detectors was operated in Small Window mode. Source products were extracted from the cleaned event files using XMMSELECT, using circular regions of radius ∼35 arcsec for the source aperture. For the EPIC-pn detector the background was always estimated from a larger region of blank sky on the same CCD as the source. This was not possible for the EPIC-MOS detectors owing to the use of Small Window mode, so for these detectors background was estimated from larger regions of blank sky on adjacent chips. As recommended, we only consider single and double patterned events for the EPIC-pn detector (PATTERN ≤ 4) and single to quadruple patterned events for the EPIC-MOS detectors (PATTERN ≤ 12), and for EPIC-pn we only consider events with FLAG = 0. Periods of high background were excluded from our analysis, and we determined the appropriate background threshold to exclude based on the technique outlined by E. Piconcelli et al. (2004), which determines the background level that maximizes the S/N for the source data (we use the full 0.3–10.0 keV EPIC bandpass for this assessment). The instrumental response files for each of the EPIC detectors were generated with RMFGEN and ARFGEN. After

performing the data reduction separately for each of the EPIC-MOS units, and confirming their consistency, the spectra from these detectors were combined using the FTOOL ADDASCASPEC for each observation.

2.3 Archival broad-band observations

In addition to these new observations, we also consider the six archival broad-band observations combining *XMM–Newton*, *Suzaku*, and *NuSTAR* reported by D. J. Walton et al. (2014, 2017a). The data reduction for these observations largely follows the process outlined in those works, but where relevant we have reprocessed the data with updated instrumental calibration files (the *Suzaku* calibration has not been updated since the latter of those works were published), and have updated the reduction of the archival *XMM–Newton* observations to also utilize the E. Piconcelli et al. (2004) technique highlighted above to maximize the S/N of the source data in the presence of any background flaring.

3 ANALYSIS

With these new observations in hand, we naturally undertook an updated timing analysis to search for any coherent pulsations that would identify Holmberg IX X-1 as another member of the ULX pulsar family. However, we did not detect any compelling signals (see Appendix A), so we still consider the nature of the accretor in Holmberg IX X-1 to be uncertain. We therefore focus our main analysis on the broad-band spectral properties of the new observations, and the spectral variability exhibited when compared to the archival observations. Our spectral analysis is performed with XSPEC (version 12.11.1; K. A. Arnaud 1996) and we fit the data by reducing the χ^2 statistic; all the data sets considered here are binned to have a minimum S/N of 5 to facilitate this. All our spectral models include absorption from the column through our own Galaxy in the direction of Holmberg IX X-1 ($N_{\rm H,Gal} = 5.5 \times 10^{20}$ cm^{-2}; HI4PI Collaboration 2016), in addition to neutral absorption more local to the source. Both are modelled with the TBABS absorption code (J. Wilms, A. Allen & R. McCray 2000), and we adopt the solar abundances quoted in that work as well as the absorption cross-sections of D. A. Verner et al. (1996), as recommended for this model. Finally, unless stated otherwise, parameter uncertainties are given at the 90 per cent level (i.e. $\Delta\chi^2 = 2.71$).

Of the five new observations (epochs 7–11), the last two show relatively similar spectra to prior broad-band observations of Holmberg IX X-1; epoch 10 is reasonably similar to the 'high' state observation discussed in D. J. Walton et al. (2017a) (epoch 2), and epoch 11 is similar to the 'medium' state observations discussed in that same work (epochs 1, 3, and 6). However, as noted above, epochs 7–9 are distinctly different from prior broad-band observations (although are themselves all relatively similar to one another). The high-energy flux – which previously appeared to be remarkably stable across epochs 1–6 despite the strong variations seen below ∼10 keV – has significantly collapsed in these three observations. We show a comparison of the broad-band spectrum seen from the first of these (epoch 7) with the three prior representative broad-band spectra highlighted by D. J. Walton et al. (2017a) in Fig. 2. At low energies (below ∼2 keV) these new spectra initially appear to be similar to the high state data, but they then peak at lower energy (∼3–4 keV) before falling away very sharply; the source is generally not detected above ∼20 keV in these observations (in contrast to earlier observations, in which the source was detected up to ∼40 keV).
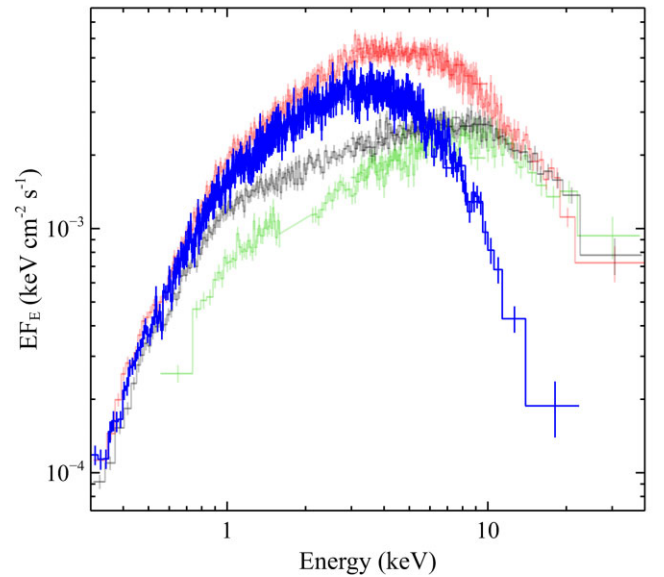

Figure 2. The broad-band spectrum of one of the new soft state observations of Holmberg IX X-1 (epoch 7; solid blue), compared to the three broad-band spectra highlighted by D. J. Walton et al. (2017a) that are representative of the archival observations (epochs 1, 2, and 4; faded black, red, and green, respectively). For clarity, we only show the *NuSTAR* data from FPMA along with one of the accompanying soft X-ray detectors (either the EPIC-pn data for *XMM–Newton* or the FI XIS data for *Suzaku*). Of the four other new broad-band epochs presented in this work, epochs 8 and 9 are similar to epoch 7 (blue), epoch 10 is similar to epoch 2 (red), and epoch 11 is similar to epoch 1 (black). All the data have been unfolded through the same model, which is simply constant with energy, and the data have been further rebinned for visual purposes.

3.1 A new broad-band spectral state

In order to characterize this new 'soft' broad-band spectral state[2] we focus initially on the data from epoch 7, as the first of these three relevant observations and also the one with the highest S/N *NuSTAR* data. Given the significant collapse in the high-energy flux seen during this soft state, we initially consider a model that consists of just the two thermal components highlighted previously. Specifically, we start by combining the DISKBB and DISKPBB models (K. Mitsuda et al. 1984; S. Mineshige et al. 1994), as has become fairly standard within the recent literature. DISKBB formally describes the thermal emission from a standard geometrically thin accretion disc (which should be present outside of the 'spherization' radius, $R_{\rm sp}$, the point at which the total luminosity integrated from the outer disc inwards reaches the Eddington luminosity; N. I. Shakura & R. A. Sunyaev 1973), but its thermal nature likely means it is also well suited to describing any cooler emission from an optically thick wind; this model is simply characterized by an inner disc temperature ($T_{\rm in}$) and a normalization. The DISKPBB model is slightly more complex as it also allows the radial temperature index (p) to vary as an additional free parameter, and so is often used as a simple approximation of a thicker super-Eddington accretion disc (which would be expected

---

[2]Note that we are using this nomenclature purely to distinguish these new observations of Holmberg IX X-1 from the broad-band spectra reported previously (D. J. Walton et al. 2014, 2017a); we are not implying that during these observations Holmberg IX X-1 is in the classical soft state seen in sub-Eddington X-ray binaries (e.g. R. A. Remillard & J. E. McClintock 2006).

Table 2. Key parameters obtained for the various continuum model fits to the high-flux data available for Holmberg IX X-1.

Model component	Parameter		Epoch 7	Stacked soft state
Continuum model: DISKBB + DISKPBB				
TBABS	N_H	$(10^{21}$ cm$^{-2})$	$1.1^{+0.2}_{-0.1}$	1.2 ± 0.1
DISKBB	T_{in}	(keV)	0.32 ± 0.06	$0.31^{+0.04}_{-0.03}$
	Norm		$7.0^{+8.0}_{-3.2}$	$9.9^{+4.9}_{-3.0}$
DISKPBB	T_{in}	(keV)	$1.56^{+0.03}_{-0.04}$	1.44 ± 0.02
	p		$0.69^{+0.05}_{-0.03}$	0.71 ± 0.03
	Norm		0.09 ± 0.02	0.13 ± 0.02
χ^2/DoF			1995/1870	2529/2372
Continuum model: DISKBB + DISKPBB⊗SIMPL				
TBABS	N_H	$(10^{21}$ cm$^{-2})$	1.0 ± 0.1	1.1 ± 0.1
DISKBB	T_{in}	(keV)	$0.39^{+0.02}_{-0.05}$	$0.34^{+0.03}_{-0.02}$
	Norm		$7.5^{+3.3}_{-1.9}$	$9.8^{+2.4}_{-1.0}$
DISKPBB	T_{in}	(keV)	$1.31^{+0.09}_{-0.04}$	$1.34^{+0.05}_{-0.01}$
	p		>0.81	$0.80^{+0.16}_{-0.06}$
	Norm		$0.38^{+0.06}_{-0.16}$	$0.22^{+0.01}_{-0.06}$
SIMPL	Γ		>2.8	>3.0
	f_{sc}	(per cent)	15^{+4}_{-9}	6^{+2}_{-5}
χ^2/DoF			1957/1868	2502/2370
Continuum model: DISKBB + DISKPBB + CUTOFFPL				
TBABS	N_H	$(10^{21}$ cm$^{-2})$	$1.0^{+0.2}_{-0.1}$	1.1 ± 0.1
DISKBB	T_{in}	(keV)	$0.38^{+0.05}_{-0.06}$	0.34 ± 0.03
	Norm		$7.1^{+3.9}_{-2.0}$	$9.5^{+3.5}_{-2.3}$
DISKPBB	T_{in}	(keV)	$1.39^{+0.07}_{-0.04}$	1.37 ± 0.03
	p		>0.75	$0.78^{+0.09}_{-0.05}$
	Norm		$0.25^{+0.06}_{-0.08}$	$0.20^{+0.06}_{-0.05}$
CUTOFFPL	Γ		0.59[a]	0.59[a]
	E_{cut}	(keV)	7.9[a]	7.9[a]
	Norm	(10^{-5})	$3.5^{+0.7}_{-1.0}$	$1.4^{+0.4}_{-0.5}$
χ^2/DoF			1962/1869	2504/2371

[a]Parameter was fixed during the fit; these are based on the average parameters found for the accretion columns in the known ULX pulsars via phase-resolved spectroscopy (see text).

interior to R_{sp}, provided that the disc has not been truncated outside of this point should the accretor be a magnetic neutron star).

This model fits the broad-band data quite well in a statistical sense, with $\chi^2 = 1995$ for 1870 degrees of freedom (DoF), but despite the overall collapse of the high-energy flux there are still excess residuals seen at the highest energies probed by *NuSTAR* during this epoch (~ 20 keV, see Fig. 2). We present the best-fitting spectral parameters in Table 2 and show the data/model ratio in Fig. 3. The high-energy excess seen in the ratio plot is qualitatively similar to what is seen in other ULXs with high-quality broad-band coverage when fit with thermal models (including previous observations of Holmberg IX X-1), and suggests that even during this epoch the high-energy spectrum does not fall away with a thermal/Wien spectrum.

We therefore also explore a couple of additional models where a third, high-energy continuum component is included as well, intended to represent both the Compton up-scattering corona and accretion column possibilities discussed above (as the nature of the accretor in Holmberg IX X-1 is still not known). For the former
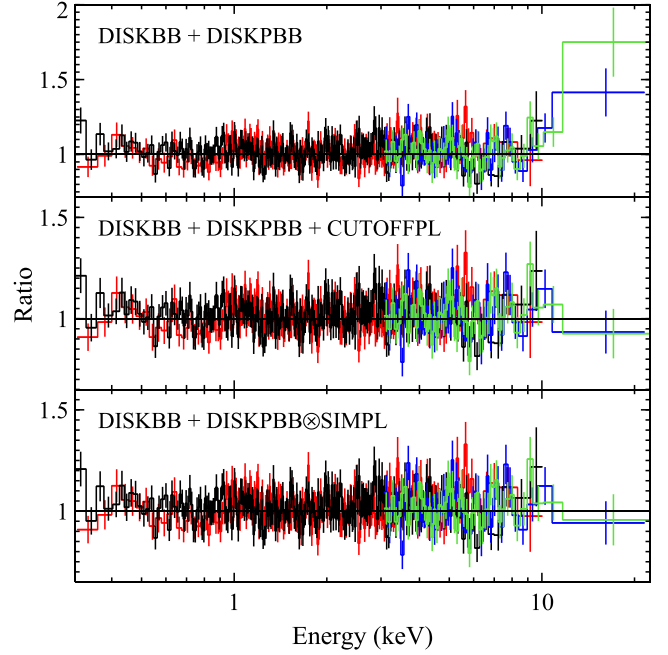

Figure 3. Data/model ratios for the continuum models applied to the broad-band data from epoch 7 (one of the observations showing the new 'soft' state revealed by our recent broad-band campaign) presented in Table 2. Even though the high-energy flux has largely collapsed here, models that only include thermal emission (top) still leave statistically significant residuals at the highest energies seen by *NuSTAR*, suggesting there is still some small contribution from a higher energy component during this epoch (modelled as an accretion column and an up-scattering corona in the middle and bottom panels, respectively). Here, the EPIC-pn, EPIC-MOS, FPMA, and FPMB data are shown in black, red, green, and blue, respectively, and the data have again been further rebinned for visual purposes.

scenario, we use the SIMPL convolution model (J. F. Steiner et al. 2009), which adds on a high-energy power-law continuum to a given input emission component, and mimics a scattering process by assuming the photon number is conserved when this additional continuum is generated. This is applied to the DISKPBB component, and is characterized with a photon index (Γ) and a scattered fraction (f_{sc}, which essentially acts as a normalization for the power-law tail). For the latter scenario, following D. J. Walton et al. (2020) we approximate the accretion column with a CUTOFFPL component (i.e. a power law with an exponential high-energy cut-off) with parameters $\Gamma = 0.59$ and $E_{cut} = 7.9$ keV; this is based on the average spectral form of the accretion column seen in the other ULX pulsars for which phase-resolved spectroscopy has been possible (M. Brightman et al. 2016; D. J. Walton et al. 2018b, c, a); only the normalization of this component is free to vary.

Both models provide similarly good fits to the data; the corona model gives χ^2/DoF = 1957/1868 and the accretion column model gives χ^2/DoF = 1962/1869. Furthermore, in both cases the improvements in the fit are sufficiently large to indicate that a high-energy component is still significantly detected during this epoch; the corona model gives an improvement of $\Delta\chi^2 = 38$ for two extra free parameters, and the accretion column model gives an improvement of $\Delta\chi^2 = 34$ for one extra free parameter. In the former case the photon index is very steep ($\Gamma > 2.8$), similar to the results found when a similar model is applied to other ULXs (e.g. E. S. Mukherjee et al. 2015; D. J. Walton et al. 2015a), and also consistent with the high-energy photon indices found in the archival *NuSTAR* observations

of Holmberg IX X-1 (D. J. Walton et al. 2014, 2017a; W. Luangtip et al. 2016; A. Gúrpide et al. 2021). The scattered fraction, however, is significantly lower for the epoch 7 data than for the archival *NuSTAR* observations. In the accretion column model, the flux of this component is also significantly lower than the archival *NuSTAR* observations; for comparison, the 2–10 keV flux of the CUTOFFPL component here is $3.6^{+0.8}_{-1.1} \times 10^{-13}$ erg cm^{-2} s^{-1} (compared with $\sim 2 \times 10^{-12}$ erg cm^{-2} s^{-1} when this model is applied to the archival data; D. J. Walton et al. 2018c).

One oddity with the results for this new soft state when compared with the archival broad-band data is that the radial temperature index is fairly steep in both of our three-component models ($p > 0.75$). For comparison, a standard thin disc is should have $p = 0.75$, and a super-Eddington disc is broadly expected to have $p < 0.75$, as found in the similar fits to the archival data. This implies that the model is trying to make the DISKPBB component much more peaked than in the archival fits. Given this, we explore whether two thermal components are really needed in this soft state, or whether this could be a result of the fit trying to model a single broad thermal component with two different components, and remove the cooler DISKBB component from both of the corona and the accretion column models. In both cases, doing so degrades the fit by $\Delta\chi^2 \sim 45$ for two fewer free parameters, suggesting that a dual-thermal continuum below 10 keV is still statistically preferred. It is also notable that the absorption column local to Holmberg IX X-1 inferred here is lower than the average column found across the archival observations of Holmberg IX X-1 where similar models have been applied ($N_H \sim 1.5 \times 10^{21}$ cm^{-2}; J. M. Miller et al. 2013; D. J. Walton et al. 2017a). This could impact the radial temperature index inferred for the DISKPBB component as this parameter primarily impacts the slope of its spectrum below the peak temperature. Indeed, if we force this column density to be 1.5×10^{21} cm^{-2} we do find the best-fitting values shifts to $p \sim 0.7$ in both models (although the quality of the fit does degrade slightly).

We have also repeated this analysis after stacking all the soft state data together (i.e. co-adding epochs 7–9 using ADDASCASPEC). These results are also presented in Table 2, and are broadly similar to the results found for epoch 7 by itself. The improvement in the fit after including an additional high-energy component still suggests this component is present in the data, but remains broadly at the same level as when considering epoch 7 alone ($\Delta\chi^2 \sim 25$–30). This is because the high-energy flux in epochs 8 and 9 is even weaker than in epoch 7, and so the preference for this third component is driven almost exclusively by the data from this epoch. In contrast, the preference for two thermal components becomes even stronger in the stacked data; removing the DISKBB component results in an even larger degradation in the fit ($\Delta\chi^2 > 100$).

3.2 Luminosity versus temperature

In order to further explore the long-term behaviour of Holmberg IX X-1, we now fit the two main continuum models discussed above (i.e. for non-magnetic and magnetic accretors) to the full set of broad-band observations. Here, we follow the analysis presented in D. J. Walton et al. (2020) of the multi-epoch broad-band data available for another ULX, NGC 1313 X-1. In short, we fit these two continuum models to all the available broad-band spectra simultaneously. In both cases, we assume that the neutral absorption column is the same for all observations (e.g. J. M. Miller et al. 2013), although this is globally free to vary. For the magnetic accretor model, we again assume the same spectral form for the accretion column as in Section 3.1 (a CUTOFFPL model with $\Gamma = 0.59$ and $E_{cut} = 7.9$ keV,

based on the average spectral shape of the accretion columns in the known ULX pulsars). For the non-magnetic accretor model with an up-scattering corona, we again use the SIMPL model, and we assume a common photon index for all observations (the high-energy spectra are very similar in eight out of the eleven broad-band observations, and the one case during the softer state where this higher energy component is seen is also consistent with having the same slope as in the other observations), although again this is free to vary globally.

Both of these continuum models provide excellent global fits to the multi-epoch broad-band data; the non-magnetic accretor model gives a total $\chi^2/\text{DoF} = 21696/21489$, while the magnetic accretor model gives a total $\chi^2/\text{DoF} = 21705/21490$. The best-fitting parameters for both models are given in Table 3.

Given the similarity of the behaviour in the archival data for Holmberg IX X-1 and that seen from NGC 1313 X-1, we are particularly interested in the behaviour of the DISKPBB component included in both models in the luminosity–temperature plane. Following D. J. Walton et al. (2020), we compute the luminosities of this component over a broad enough band to be considered bolometric (0.001–100 keV), and plot the luminosity–temperature evolution for both models in Fig. 4. For comparison, in addition to the data we show example trends following $L \propto T^4$ and $L \propto T^2$. The former scaling is expected for blackbody emission from with a constant emitting area, and the latter is predicted by K.-y. Watarai et al. (2000) for an advection-dominated super-Eddington disc with a constant inner radius around a black hole (the flatter relation comes about because some of the radiation emitted by the disc becomes trapped within it and is carried over the event horizon instead of escaping to infinity).

The two models show different behaviours for Holmberg IX X-1, relating in particular to the new, soft state highlighted above. In the magnetic accretor model, the higher temperature observations do show evidence of following a coherent luminosity–temperature relation which appears to be slightly better described with $L \propto T^4$ than with $L \propto T^2$. However, the lower temperature observations (including the soft state) do not show a single, well-defined trend. One could choose to connect the two lower temperature observations in which the high-energy emission is at its normal level (epochs 2 and 10), in which case these data would roughly follow an $L \propto T^4$ trend with the soft state observations (which cluster together) appearing as outliers. Alternatively, one could choose to connect the soft state observations with the brightest broad-band observation to date (epoch 2), in which case these data would roughly follow an $L \propto T^2$ trend with epoch 10 being an outlier. Given the significant difference in high-energy flux seen in the soft state observations, the former may be the more natural scenario in this case. Nevertheless, it is worth nothing that, while advection over a horizon is not possible for neutron star accretors, if the accretor is magnetized with the disc truncated at the magnetosphere it is still possible to have luminosity–temperature relations that are flatter than $L \propto T^4$, as the radius of the magnetosphere is generally expected to vary with accretion rate in an inverse manner (although there may be some range of accretion rates where this is not the case; A. Chashkina et al. 2019).

In contrast, the non-magnetic accretor model does seem to show two well-defined luminosity–temperature tracks, similar to the results seen for NGC 1313 X-1 (D. J. Walton et al. 2020). In this case, both the higher and lower temperature trends seem to be slightly better described with $L \propto T^2$ than $L \propto T^4$, but ultimately the data would appear to be consistent with both possibilities. The key difference here is the use of the SIMPL model to generate the highest energy emission. In contrast to the use of the CUTOFFPL model in the magnetic accretor model, which is an additive component that is not formally coupled to the DISKPBB component of interest here, SIMPL

Table 3. Best-fitting parameters from the eleven broad-band spectra currently available for Holmberg IX X-1 for the models assuming a non-magnetic and a magnetic accretor, respectively.

Model Component	Parameter	1	2	3	4	5	6	7	8	9	10	11
							Broad-band epoch					
		Non-magnetic accretor model: TBABS× (DISKBB + DISKPBB ⊗ SIMPL)										
TBABS	$N_{\rm H,int}$[a] (10^{21} cm^{-2})	1.34 ± 0.05	–	–	–	–	–	–	–	–	–	–
DISKBB	$T_{\rm in}$ (keV)	0.31 ± 0.01	0.27 ± 0.03	$0.27^{+0.02}_{-0.03}$	$0.31^{+0.04}_{-0.02}$	$0.31^{+0.03}_{-0.02}$	$0.45^{+0.07}_{-0.08}$	0.29 ± 0.03	0.31 ± 0.03	0.28 ± 0.03	0.33 ± 0.02	0.33 ± 0.02
	Norm	$9.6^{+2.0}_{-1.6}$	$14.3^{+6.9}_{-5.5}$	$26.1^{+12.2}_{-8.3}$	$9.0^{+3.8}_{-2.6}$	$9.3^{+3.8}_{-2.6}$	$1.0^{+0.9}_{-0.7}$	$18.4^{+4.8}_{-4.1}$	$15.6^{+6.2}_{-5.3}$	$17.6^{+6.2}_{-5.3}$	$11.2^{+2.7}_{-2.1}$	$6.5^{+2.1}_{-1.7}$
DISKPBB	$T_{\rm in}$ (keV)	$3.0^{+0.3}_{-0.6}$	$1.6^{+0.1}_{-0.3}$	$2.7^{+0.7}_{-0.4}$	$2.4^{+0.7}_{-0.2}$	$2.3^{+0.5}_{-0.2}$	3.0 ± 0.7	$1.41^{+0.05}_{-0.06}$	$1.34^{+0.04}_{-0.06}$	$1.38^{+0.04}_{-0.05}$	$1.18^{+0.17}_{-0.11}$	$3.2^{+0.5}_{-0.6}$
	p	$0.579^{+0.005}_{-0.004}$	0.67 ± 0.02	$0.59^{+0.02}_{-0.01}$	$0.65^{+0.04}_{-0.02}$	$0.68^{+0.04}_{-0.02}$	0.58 ± 0.02	$0.75^{+0.09}_{-0.05}$	$0.75^{+0.02}_{-0.07}$	$0.70^{+0.06}_{-0.04}$	>0.72	0.57 ± 0.01
	Norm (10^{-3})	$2.5^{+0.4}_{-0.8}$	102^{+144}_{-31}	$3.7^{+3.0}_{-2.2}$	$6.1^{+2.7}_{-3.7}$	$8.8^{+4.3}_{-3.3}$	$1.9^{+1.4}_{-1.0}$	168^{+86}_{-45}	198^{+118}_{-52}	145^{+57}_{-32}	303^{+379}_{-145}	$1.6^{+1.3}_{-0.6}$
SIMPL	Γ[a]	$3.53^{+0.13}_{-0.12}$	–	–	–	–	–	–	–	–	–	–
	$f_{\rm scat}$ (per cent)	>38	>42	>37	>48	>58	>27	9^{+2}_{-3}	<4	<3	>77	>15
χ^2/DoF		21696/21489										
		Magnetic accretor model: TBABS× (DISKBB + DISKPBB + CUTOFFPL)										
TBABS	$N_{\rm H,int}$[a] (10^{21} cm^{-2})	$1.41^{+0.07}_{-0.03}$	–	–	–	–	–	–	–	–	–	–
DISKBB	$T_{\rm in}$ (keV)	$0.32^{+0.01}_{-0.02}$	0.25 ± 0.04	0.26 ± 0.03	$0.32^{+0.04}_{-0.03}$	$0.32^{+0.04}_{-0.03}$	$0.49^{+0.20}_{-0.07}$	$0.27^{+0.03}_{-0.02}$	$0.30^{+0.02}_{-0.03}$	0.26 ± 0.03	0.31 ± 0.02	$0.34^{+0.03}_{-0.02}$
	Norm	$8.0^{+1.9}_{-1.4}$	$14.0^{+12.6}_{-7.0}$	$25.3^{+16.1}_{-8.2}$	$9.2^{+3.7}_{-2.6}$	$9.3^{+3.7}_{-2.6}$	$0.8^{+1.4}_{-0.7}$	$21.5^{+8.5}_{-5.2}$	$18.1^{+5.9}_{-4.1}$	$21.4^{+10.2}_{-6.6}$	$11.2^{+3.5}_{-2.4}$	$5.6^{+2.7}_{-1.9}$
DISKPBB	$T_{\rm in}$ (keV)	2.7 ± 0.2	1.90 ± 0.04	$2.6^{+0.5}_{-0.3}$	2.4 ± 0.4	$2.2^{+0.4}_{-0.3}$	$2.7^{+0.7}_{-0.5}$	1.47 ± 0.05	$1.35^{+0.05}_{-0.04}$	1.39 ± 0.04	1.65 ± 0.08	$2.8^{+0.7}_{-0.4}$
	p	0.55 ± 0.01	0.63 ± 0.01	0.56 ± 0.02	$0.64^{+0.13}_{-0.05}$	>0.66	0.55 ± 0.03	$0.72^{+0.06}_{-0.04}$	$0.73^{+0.09}_{-0.05}$	0.69 ± 0.04	$0.73^{+0.08}_{-0.05}$	0.54 ± 0.01
	Norm (10^{-3})	$2.1^{+0.7}_{-0.5}$	44^{+6}_{-5}	$2.3^{+2.0}_{-1.1}$	$4.0^{+7.0}_{-2.2}$	$8.1^{+14.9}_{-4.8}$	$1.8^{+2.6}_{-1.0}$	131^{+45}_{-29}	177^{+77}_{-45}	136^{+43}_{-27}	72^{+36}_{-20}	$1.8^{+1.5}_{-0.9}$
CUTOFFPL	Γ	0.59[b]	–	–	–	–	–	–	–	–	–	–
	$E_{\rm fold}$ (keV)	7.9[b]	–	–	–	–	–	–	–	–	–	–
	Norm (10^{-4})	2.4 ± 0.2	2.3 ± 0.1	$2.6^{+0.3}_{-0.4}$	$2.5^{+0.2}_{-0.3}$	$2.5^{+0.2}_{-0.3}$	$2.3^{+0.3}_{-0.6}$	0.28 ± 0.09	<0.12	<0.09	2.1 ± 0.2	$2.0^{+0.4}_{-0.9}$
χ^2/DoF		21705/21490										
$F^{\rm obs}_{0.3-1.0}$[c] (10^{-12} erg cm^{-2} s^{-1})		1.15 ± 0.02	1.63 ± 0.02	1.15 ± 0.06	0.69 ± 0.03	0.61 ± 0.03	0.84 ± 0.05	1.34 ± 0.03	1.39 ± 0.04	1.37 ± 0.04	1.12 ± 0.03	1.12 ± 0.03
$F^{\rm obs}_{1.0-10.0}$[c]		9.7 ± 0.1	19.2 ± 0.2	8.9 ± 0.2	7.1 ± 0.1	6.8 ± 0.1	8.3 ± 0.2	12.2 ± 0.2	11.1 ± 0.2	10.9 ± 0.2	13.1 ± 0.2	8.9 ± 0.2
$F^{\rm obs}_{10.0-40.0}$[c]		3.5 ± 0.1	3.4 ± 0.1	3.4 ± 0.1	3.1 ± 0.1	3.1 ± 0.1	3.1 ± 0.2	0.55 ± 0.08	0.20 ± 0.05	$0.19^{+0.05}_{-0.03}$	2.7 ± 0.1	2.9 ± 0.2
$F^{\rm obs}_{0.3-40.0}$[c]		14.3 ± 0.2	24.3 ± 0.2	13.5 ± 0.3	10.9 ± 0.2	10.5 ± 0.2	12.2 ± 0.3	14.1 ± 0.3	12.7 ± 0.3	12.5 ± 0.3	16.9 ± 0.3	12.9 ± 0.3
$L^{\rm int}_{0.3-40.0}$[d] (10^{40} erg s^{-1})		2.55 ± 0.04	4.21 ± 0.05	2.43 ± 0.06	1.87 ± 0.04	1.78 ± 0.04	2.14 ± 0.06	2.56 ± 0.06	2.36 ± 0.06	2.33 ± 0.06	2.92 ± 0.05	2.34 ± 0.06

[a] These parameters are globally free to vary, but are linked across all epochs.

[b] These parameters are fixed to the average values seen from the pulsed emission from the currently known ULX pulsars, and are common for all epochs.

[c] The total observed flux in the full 0.3–40.0 keV band, and the 0.3–1.0, 1.0–10.0, and 10.0–40.0 keV sub-bands, respectively (consistent for both models).

[d] Absorption-corrected luminosity in the full 0.3–40.0 keV band (consistent for both models). These values assume isotropic emission, and may therefore be upper limits.
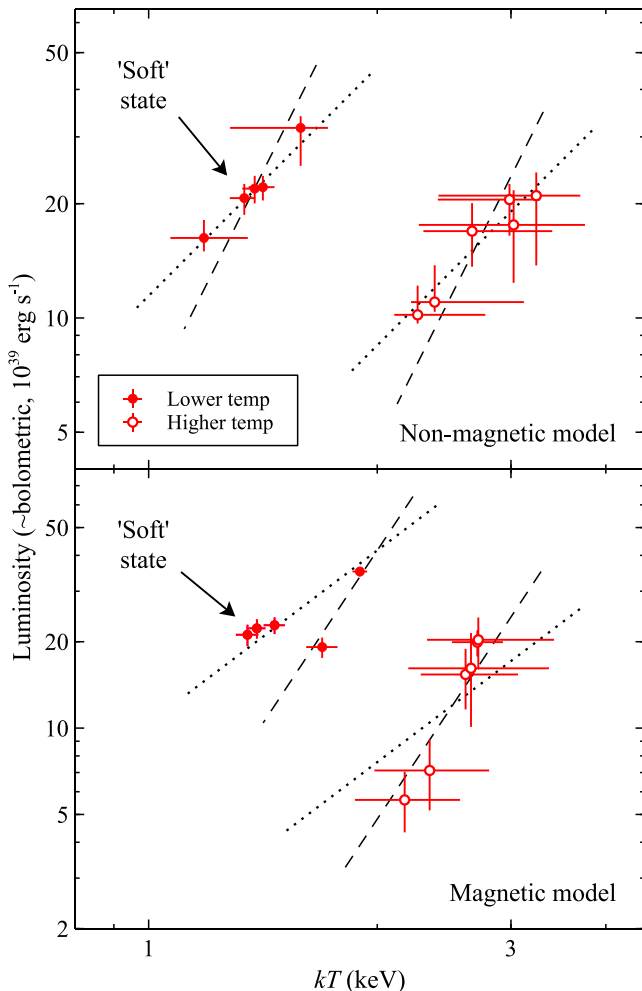
Figure 4. 0.001–100 keV (i.e. ~bolometric) luminosity vs temperature for the DISKPBB component from our multi-epoch broad-band spectral analysis of Holmberg IX X-1. Results for the models assuming the accretor is non-magnetic and magnetic are shown in the top and bottom panels, respectively. In the former case, evidence for two distinct luminosity–temperature tracks are seen, both of which are consistent with either $L \propto T^4$ (dashed lines) or $L \propto T^2$ (dotted lines), similar to the results found for NGC 1313 X-1 (D. J. Walton et al. 2020). In the latter case, the situation is less clear, with the soft state observations clearly separating themselves from the other high-flux observations in the luminosity–temperature plane. The remaining observations are consistent with there being two distinct luminosity–temperature tracks that follow $L \propto T^4$, but with only two observations on the high-flux/low-temperature track the presence of these two tracks cannot be well established for the magnetic accretor model with the current data.

assumes that every photon that contributes to the highest energy component was previously emitted by the disc. The bolometric disc flux is calculated prior to the application of the SIMPL component in our analysis. As such, the properties inferred for the high-energy continuum have a more direct impact on the properties inferred for the disc, resulting in the different luminosity–temperature behaviour for the lower temperature observations when compared to the magnetic accretor model, given the strong changes in the high-energy flux during the soft state observations.

The direct coupling between the SIMPL and DISKPBB components described above not only impacts the best-fitting properties inferred for the disc, but also results in stronger parameter degeneracies than for the magnetic accretor model, and thus larger overall parameter

uncertainties (the exceptions being the soft state observations, where the high-energy continuum is sufficiently weak that the degeneracies with the disc properties are minimized). However, with regards to assessing the presence of the luminosity–temperature trends with this model, these uncertainties are likely slightly misleading, as they are partially driven by uncertainties in the high-energy photon index, which is strongly connected to the inferred disc properties. This is treated as being common for all observations, and as such changes in Γ cause almost all the observations to change in tandem. This degeneracy therefore expands the formal parameter uncertainties on the disc properties for almost all the observations, but does not remove the need for the relative variations between epochs that drive the overall presence of the luminosity–temperature trends seen in Fig. 4. Indeed, we have confirmed that fixing Γ to its best-fitting value and to its ±90 per cent parameter bounds reduces the average fractional parameter uncertainties for both the luminosity and the temperature measurements in all three cases, and that two positive luminosity–temperature trends are still seen when pushing Γ to these limits.

Again following the analysis presented in D. J. Walton et al. (2020), in order to alleviate any concerns that the luminosity–temperature behaviour shown in Fig. 4 may be driven by the use of fluxes that are significantly extrapolated beyond the observed bandpass, we also re-assess the luminosity–temperature behaviour for the DISKPBB component using fluxes calculated above 1 keV instead. While there are necessarily quantitative differences in the fluxes relating to this change in bandpass, for both the models considered the same qualitative behaviour to that shown in Fig. 4 is still seen with this alternative analysis. We have also investigated relaxing the assumption that all epochs share a common column density, allowing this to vary between epochs, and again the same behaviour as shown in Fig. 4 is seen.

4 DISCUSSION

We have conducted a series of five new broad-band observations of the ULX Holmberg IX X-1, combining *XMM–Newton* and *NuSTAR*. Along with the broad-band observations available in the archive, combining *XMM–Newton*, *Suzaku*, and *NuSTAR* (epochs 1–6, reported in D. J. Walton et al. 2014, 2017a; W. Luangtip et al. 2016; A. Gúrpide et al. 2021), we therefore have a set of eleven broad-band observations of Holmberg IX X-1. Compared to these archival data sets, the first three of these new observations (epochs 7–9) show a new 'soft' state in which the hard X-ray flux, previously seen to be remarkably stable, has almost completely collapsed (see Fig. 2). The final two new observations (epochs 10 and 11) are broadly similar to the first two broad-band observations taken, and show a return to the same level of hard X-ray flux seen previously (specifically, epochs 10 and 2 are similar, while epochs 11 and 1 are similar). This recovery of the hard X-ray flux took ≲12 d.

4.1 Luminosity–temperature behaviour

The consistency of the high-energy flux seen in the archival Holmberg IX X-1 data sets has also been seen in the multi-epoch broad-band data available for the ULX NGC 1313 X-1 (D. J. Walton et al. 2020). When the NGC 1313 X-1 data were fit with what are now fairly standard (albeit still phenomenological) ULX continuum models, combining two thermal components that dominate below 10 keV and an additional high-energy continuum seen above ~10 keV (either an accretion column or an up-scattering corona), the results for the hotter thermal component separated themselves into two

groups: one with higher temperatures and lower fluxes, and one with lower temperatures and higher fluxes. However, each of these groups exhibited its own *positive* luminosity–temperature trend (i.e. luminosity increasing with temperature). As the archival broad-band observations of Holmberg IX X-1 only include one observation that would correspond to the low-temperature/high-flux group seen in NGC 1313 X-1, the original purpose of the new observations presented here was to investigate whether the hotter thermal component in Holmberg IX X-1 also showed the same complex luminosity–temperature behaviour as NGC 1313 X-1, given the other similarities in their broad-band spectral evolution.

To test this, we performed a similar, multi-epoch spectral analysis to D. J. Walton et al. (2020) on the updated broad-band data for Holmberg IX X-1. Based on these fits, there is some evidence that Holmberg IX X-1 may show the same strange luminosity–temperature behaviour as seen in NGC 1313 X-1, though the results for Holmberg IX X-1 are model dependent. The case is strongest for the non-magnetic accretor model; the results for the hotter thermal component (treated with the DISKPBB model) show two clear luminosity–temperature tracks, with all the lower temperature epochs seeming to follow a coherent trend (including the new soft-state observations). The results for the magnetic accretor model are more ambiguous; here the lower temperature observations do not show a single coherent trend. However, if the new soft-state observations are treated as being distinct to the other lower temperature observations (i.e. those where there is significant hard X-ray flux), which may not be unreasonable given the differences at higher energies, then one can interpret the remaining observations as being consistent with showing two distinct luminosity–temperature tracks similar to NGC 1313 X-1 (although there are then only two observations on the higher flux/lower temperature track). Were this to be the case, the data would seem to indicate a preference for $L \propto T^4$ trends.

The cause of this behaviour is difficult to explain, particularly given that the high-energy flux seen in the broad-band NGC 1313 X-1 data (and the majority of the broad-band Holmberg IX X-1 data) is so stable and that a relatively sharp transition between the two trends is needed in the luminosity–temperature plane. D. J. Walton et al. (2020) consider a variety of different possible scenarios, including:

(i) Changes in the degree of geometric collimation/beaming[3] experienced by the emission from the innermost regions of the disc, i.e. the regions interior to the onset of the funnel-like geometry – which results in the collimation – expected for the inner regions of super-Eddington accretion discs.

(ii) The inner disc becoming completely blocked from view, such that only the outer disc/wind is seen.

(iii) The inner disc being covered by a scattering shroud, potentially related to an ionized wind (since extreme outflows are known to be present in NGC 1313 X-1; C. Pinto et al. 2016, 2020; D. J. Walton et al. 2016a), resulting in a diminished (but non-zero) flux from these regions of the disc reaching the observer.

(iv) Changes in atmospheric effects in the disc (i.e. its colour correction factor) and/or the amount of down-scattering in the wind.

(v) Emission from distinct (e.g. radially segregated) regions of the accretion flow having different variability properties such that they each dominate the total emission at different times. These regions would likely be determined by the key radii expected for super-Eddington accretion, i.e. the inner disc radius (set by the innermost

stable circular orbit for a black hole, the neutron star surface for a non-magnetized neutron star, or the magnetospheric radius for a magnetic neutron star) and the 'spherization' radius.

However, in the end none of these possibilities were considered to offer an entirely satisfactory explanation for the broad-band data for NGC 1313 X-1. We do not repeat that discussion in detail here, and instead refer the reader to that work for a more in-depth consideration of these possibilities. However, to briefly summarize the main issues, scenarios invoking geometric changes to produce the two luminosity–temperature tracks (i.e. differences in beaming, occultation) struggled to explain the lack of corresponding variability at the highest energies, as regardless of whether this emission is associated with a scattering corona or an accretion column the general expectation is that this emitting region should be central and compact, and so should respond similarly to anything impacting the emission from the inner disc. A number of the other scenarios discussed would have implied bimodal behaviour (or at least sharp transitions) in quantities that would likely be expected to vary smoothly with accretion rate (e.g. the amount of beaming, the colour correction factor) to produce two distinct luminosity–temperature tracks.

The final possibility, invoking multiple different regions in a complex, super-Eddington disc is likely the most compelling, but here it is then also necessary to explain the further presence of the second, cooler thermal component at $\sim$0.3 keV required by the broad-band data (such that there are at least three distinct regions of the accretion flow that manifest themselves in the data, in addition to the high-energy corona/accretion column). For a magnetized neutron star accretor, one notable possibility is that the two luminosity–temperature tracks correspond to distinct thermal contributions from the super-Eddington disc interior to $R_{\rm sp}$, and the accretion curtain that connects the disc at $R_{\rm M}$ to the accretion columns, which A. A. Mushtukov et al. (2017) suggest should be optically thick. However, it is not entirely clear why the intermediate temperature regions (corresponding to the cooler of the luminosity–temperature tracks seen from the DISKPBB component) would dominate the total emission on some occasions but not on others.

While the high-energy flux from Holmberg IX X-1 has now been seen to vary significantly in these new observations, there are still at least some observations on the higher flux/lower temperature track that have equivalent high-energy flux to the observations on the higher temperature/lower flux track. As such, all the issues explaining the two luminosity–temperature tracks with geometric changes discussed in D. J. Walton et al. (2020) for NGC 1313 X-1 would still also hold for Holmberg IX X-1, despite this newly observed variability.

Ultimately, though, given the more model-dependent nature of the results found here, further broad-band observations will be required to unambiguously confirm that Holmberg IX X-1 is truly exhibiting the same luminosity–temperature behaviour as seen in NGC 1313 X-1. In particular, these observations should target periods of high overall flux where there is also significant hard X-ray flux as well (i.e. the flux above $\sim$10 keV is at its 'normal' level) in order to investigate whether these observations really show a coherent luminosity–temperature trend when the magnetic accretor model is applied.

4.2 The nature of the soft state

We focus the remainder of our discussion on the nature of the soft state, and in particular the processes that could be responsible for

---

[3]Note that while this is often referred to as 'beaming' in the literature, e.g. A. R. King (2008), it is a geometric effect that is distinct from relativistic beaming.

the collapse in the observed hard X-ray flux. We consider four main possibilities:

(i) Obscuration of the inner regions of the accretion flow by regions of the super-Eddington disc/wind residing at larger radii.

(ii) The formation of a 'scattersphere' within the funnel-like geometry expected for a super-Eddington disc/wind combination.

(iii) A transition into the propeller regime (which would specifically require a magnetized neutron star as the central accretor).

(iv) Collapse/destruction of a Compton-scattering corona.

In brief, it is not clear that either of the scattersphere or propeller scenarios offer viable explanations for the observed soft state when these data are considered in the context of the multi-epoch broadband data set now available for Holmberg IX X-1. While obscuration by a super-Eddington disc/wind could be viable under certain conditions, our current view is that a scenario involving the destruction of a Compton-scattering corona may be the most plausible interpretation (though we stress that arriving at a firm conclusion is challenging with the currently available data). More detailed discussions of the scenarios we consider to be potentially viable are presented in the following subsections for the interested reader, while the others are discussed further in Appendix B.

4.2.1 Obscuration

One possibility is that the during the first three of the new observations the innermost regions were blocked from view, preventing us from seeing the highest energy emitting regions. Given the strong remaining thermal emission, the likely obscuring medium would be regions of a geometrically thick, super-Eddington accretion disc and/or its wind at larger radii. This is conceptually similar to one of the scenarios considered above for the complex luminosity–temperature behaviour, although such an obscuration-based scenario does not ultimately seem a plausible explanation for that phenomenology. It is also analogous to the scenario often invoked to explain ULXs that transition into the 'ultrasoft' regime (now referred to as ultraluminous supersoft sources, or ULSs; e.g. R. Urquhart & R. Soria 2016; C. Pinto et al. 2017; A. D'Aì et al. 2021), although we stress that the 'soft' state seen here differs markedly to these ULSs (the observed thermal emission is still much hotter than the ~ 0.1 keV emission that characterizes ULSs, and most ULS observations exhibit luminosities around the $\sim 10^{39}$ erg s^{-1} level while the soft state observations show luminosities of $\sim 10^{40}$ erg s^{-1}).

In principle, this would be possible regardless of whether the highest energy emission originates in an up-scattering corona or an accretion column since, as noted above, both would be expected to be compact and centrally located. However, based on the spectral results from our multi-epoch analysis, this scenario would likely be more plausible for the magnetic accretor model. Obscuration of the inner regions would likely also be expected to result in an accompanying sharp drop in the temperature seen from the thermal emission, as the innermost regions of the disc would likely also be obscured in addition to the corona/accretion column. When compared to the other high-flux observations (epochs 2 and 10), evidence for such a drop is only really seen with the magnetic accretor model, while the non-magnetic accretor model seems to show a smooth, coherent luminosity–temperature trend.

Even then, though, this emitting region would need to be only partially covered during epoch 7, as while it is still much weaker, the high-energy emission component seen during most other observations is still detected during this epoch. It is unclear how plausible

such a partially covering scenario is. Furthermore, the scale-height of the disc/wind is generally expected to increase with increasing accretion rate (e.g. A. R. King 2008). For any source where we typically can view the inner regions, one would therefore generally expect the onset of such occultation to occur at the highest accretion rates observed. However, the brightest observation (epoch 2) is brighter than all of the soft state observations (both in terms of total flux and the DISKPBB flux specifically), which would naively appear to imply a higher accretion rate for epoch 2. In order for this scenario to be plausible, the soft state observations would likely have to be intrinsically brighter than even epoch 2, and only appear fainter because the most luminous inner regions are blocked from view.[4] This would have further implications for the complex luminosity–temperature behaviour observed; if the soft state is what the source looks like when the innermost regions are obscured from view, then this would offer a further argument against the presence of the two 'normal' luminosity–temperature tracks being related to similar obscuration.

4.2.2 Collapsing/disappearing corona

Should the high-energy flux come from an up-scattering corona, the observed variability could instead be related to intrinsic changes in this structure. The fraction of disc photons scattered up into the high-energy component changes significantly in this model, ranging from upwards of ~ 75 per cent (epoch 10) to less than 3 per cent (epoch 9). This would indicate that the corona has essentially collapsed during the soft state observations, before re-forming by the time of epoch 10 (~ 12 d after epoch 9, the last soft-state observation). It is particularly interesting that, despite this very large change, the intrinsic properties inferred for the DISKPBB component during all of the high-flux observations (including the soft state observations) show a single, coherent trend. Again, we note that there is no reason we are aware of that this should occur by coincidence.

An interesting comparison here may be the strange recent behaviour seen in the active galactic nucleus 1ES 1927+654. Although a long-known AGN (T. Boller et al. 2003; L. C. Gallo et al. 2013), in late 2017 this source underwent a transient outburst event during which the hard X-ray corona was destroyed sometime in mid 2018, leaving an extremely soft, vaguely thermal spectrum with a temperature of ~ 100 eV and essentially no flux above $\sim$a few keV. Continued monitoring showed that the corona had begun to re-form by late 2018 and the source eventually reached X-ray luminosities significantly brighter than its pre-outburst state (although it has since returned to comparable levels; C. Ricci et al. 2020; M. Masterson et al. 2022). The cause for this outburst behaviour is not known, but it is speculated that this may have been triggered by a rare example of a tidal disruption event (TDE) in an existing AGN. TDEs are often thought to result in super-Eddington accretion, and indeed, at its peak the X-ray flux in just the 0.3–10.0 keV band alone

---

[4]Although we do not report on this analysis in full here, we note that we have also inspected the integrated soft state data from the *XMM–Newton* Reflection Grating Spectrometer (RGS; J. W. den Herder et al. 2001) to check for any ionized absorption that may further support this scenario. We do not find any notable evidence for such absorption, but stress that these data are not particularly sensitive; the individual *XMM–Newton* exposures taken during this state are short, and the situation is further exacerbated by the technical issue that occurred during epoch 9, as this also resulted in the loss of the RGS data from that epoch too, meaning there is only ~ 43 ks good RGS exposure covering the soft state. Deeper exposures targeting this state will be required to meaningfully perform meaningful searches for such absorption.

reached the Eddington limit for the $10^6\,M_\odot$ black hole this source is expected to host (C. Ricci et al. 2020), implying that the overall accretion rates were at times super-Eddington. Interestingly, during its peak fluxes the re-formed corona in 1ES 1927+654 exhibited a very steep spectrum ($\Gamma \sim 3$), somewhat similar to the coronal spectrum inferred here. The time-scale over which the corona was re-created in 1ES 1927+654 ($\sim$100 d) would easily fit in the $\sim$12-d period between epochs 9 and 10 when scaled from a $\sim 10^6\,M_\odot$ black hole to e.g. a $10\,M_\odot$ black hole, although the duration for which the corona was absent in Holmberg IX X-1 would appear to be much longer than for 1ES 1927+654 (again when scaled by the mass).

The exact process by which the corona was destroyed in 1ES 1927+654 is not well known, but given the long-term variability seen from Holmberg IX X-1 (Fig. 1) we cannot invoke anything conceptually similar to a TDE here. If these two collapses in flux really are similar then it would therefore seem more likely that they are somehow related to the high/super-Eddington rates of accretion in both sources, as opposed to dynamical processes relating to a TDE event. C. Ricci et al. (2020) speculate that the destruction of the corona in 1ES 1927+654 is related to the destruction of the innermost accretion disc, which would normally support the X-ray corona (perhaps magnetically). However, we would expect such a sudden change in the disc properties to manifest itself in the luminosity–temperature plane. For Holmberg IX X-1 we do not see any evidence for this when the high-energy emission is modelled as an up-scattering corona. One could perhaps argue that the inner disc was initially destroyed along with the corona in Holmberg IX X-1, but had since re-formed prior to epoch 7, as this may have to occur prior to the main recovery of the corona. However, the detection of the weak high-energy flux during epoch 7 may suggest that we are catching the end of the destruction process, and again there are no major differences between the disc properties during this epoch and the other soft state observations. This may instead imply that there is a way of destroying the corona without significantly impacting the disc. Alternatively, the re-formation of the corona may just not be an entirely smooth process, with epoch 7 representing something like an initial, failed attempt before the more sustained restoration occurred later on (between epochs 9 and 10).

One speculative possibility is that the collapse of the corona is somehow related to ballistic jet ejections. During their outbursts, 'normal' low-mass X-ray binaries are known to launch transient, ballistic jet ejecta as they approach luminosities close to their Eddington limits (e.g. S. Corbel et al. 2002; J. A. Tomsick et al. 2003; S. Corbel et al. 2005; J. F. Steiner, J. E. McClintock & M. J. Reid 2012). A small number of ULXs are also known to exhibit similar transient ejections (M. J. Middleton et al. 2013; D. Cseh et al. 2014, 2015), and Holmberg IX X-1 would appear to be among this number.[5] If these ejection events can 'clear out' the corona (at least on occasion), then this may offer a means to temporarily remove the corona for some period of time after they occur. It is worth noting that these transient jet events are often accompanied by strong X-ray flares (e.g. J. E. McClintock et al. 2009; J. F. Steiner et al. 2011; D. J. Walton et al. 2017b), and there are no

obvious events like this in the *Swift* monitoring immediately prior to the soft state observations. However, the flares associated with these jet ejection events typically reach $\sim$Eddington or mildly super-Eddington luminosities. It is therefore not clear whether similar flares would be detectable for a source already radiating at highly super-Eddington levels. Furthermore, these flares/flaring periods can be very brief, and so even if flaring to even higher luminosities should have occurred, this could easily have been missed by the $\sim$weekly *Swift* monitoring cadence.

Given all of these potential connections, and the coherent luminosity–temperature relation implied by this model for all the high-flux observations, we speculate that a scenario along these lines (whereby an up-scattering corona is somehow physically destroyed) may be the most plausible explanation for this new soft state in Holmberg IX X-1. However, we stress that an obscuration-related scenario cannot be excluded under the right circumstances, and that this does not shed any further light on the fact that there seem to be two distinct luminosity–temperature trends seen from the hotter thermal component in this spectral model.

5 *HEX-P* SIMULATIONS

Although we may not have a satisfactory picture for the spectral evolution exhibited by Holmberg IX X-1 at the current time, neither in terms of observationally establishing whether Holmberg IX X-1 really exhibits the two distinct luminosity–temperature tracks similar to NGC 1313 X-1 nor understanding the nature of the new 'soft' state revealed here, addressing these issues is likely to play a key role in establishing our detailed understanding of super-Eddington accretion. Such work requires continued observations to build up a larger multi-epoch broad-band data set, particularly targeting the 'normal' high-flux state. For Holmberg IX X-1 there is plenty of scope to explore this issue further with additional broad-band observations with our current facilities (i.e. further coordinated observations with, e.g. *XMM–Newton* and *NuSTAR*). Assuming that similar behaviour to NGC 1313 X-1 really is present in Holmberg IX X-1 as well, as is tentatively hinted by the current broad-band observations, going on to further establish whether this is common among the ULX population will also be of significant importance. However, building the multi-epoch broad-band data sets necessary to investigate this for a population of sources would require a vast amount of coordinated exposure with our current facilities.

The recently-proposed *HEX-P* (K. K. Madsen et al. 2024) will offer simultaneous broad-band coverage (bandpass of $\sim$0.3–80.0 keV) with unprecedented hard X-ray sensitivity (at least a factor of four better than *NuSTAR* over their common energy range), and would thus be ideally suited for such work. In order to illustrate this, we simulate a multi-epoch set of *HEX-P* observations of Holmberg IX X-1, assuming for illustration that the DISKPBB component in this source does indeed exhibit two distinct luminosity–temperature trends, each of which follows $L \propto T^4$. For simplicity, we focus on the magnetic accretor model for these simulations, and we simulate the same number and make-up of *HEX-P* observations as the overall number of broad-band observations as are currently available: six in the lower flux/higher temperature group and five in the higher flux/lower temperature group (11 in total). The lower flux/higher temperature simulations span temperatures of 2–3 keV, while the higher flux/lower temperature simulations span temperatures of 1.65–2.15 keV, while typical parameters for the cooler DISKBB component were adopted based on the results presented earlier, and the hard X-ray flux (10–40 keV, which sets the normalization of the highest energy

---

[5]Infrared (IR) emission consistent with a jet was originally reported by R. P. Dudik et al. (2016), and then further investigation of the full, multi-epoch *Spitzer* data showed that this corresponded to a brief, transient period of IR activity (R. M. Lau et al. 2019). Recent constraints on the presence of a compact radio source associated with Holmberg IX X-1 further confirm that the jet activity must be transient (C. T. Berghea et al. 2020).
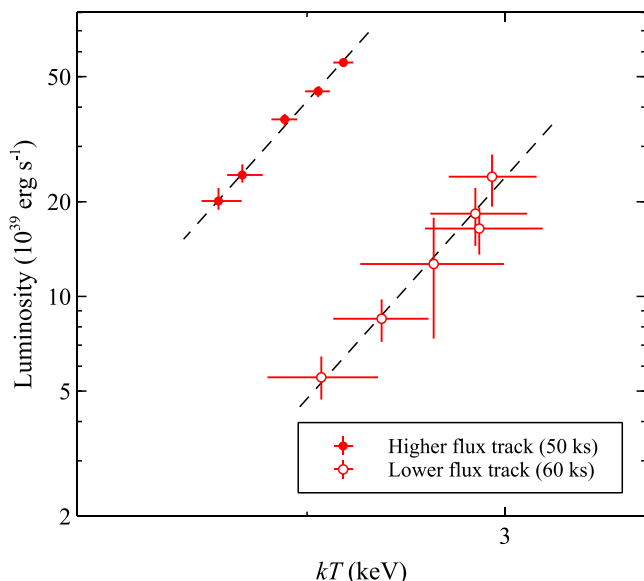
Figure 5. Simulated *HEX-P* luminosity–temperature constraints for the DISKPBB component. For simplicity, we focus only on the magnetic accretor model here, and we also explicitly assume that Holmberg IX X-1 does exhibit two distinct luminosity–temperature tracks that each follow $L \propto T^4$ when the source has a 'normal' hard X-ray flux (i.e. the hard X-ray flux seen in all observations apart from the new soft state discovered here), similar to the results seen from NGC 1313 X-1. In total 11 *HEX-P* observations are simulated (matching the number of broad-band observations currently in the archive for Holmberg IX X-1), five in the higher flux/lower temperature track (50 ks exposurs) and six in the lower flux/higher temperature track (60 ks exposures), with a total exposure of ∼600 ks. The luminosity–temperature constraints from these *HEX-P* observations would be either equivalent or superior to the current constraints that combine ∼1.6 Ms of observing time from *XMM–Newton*, *Suzaku*, and *NuSTAR*.

component) was assumed to be 3×10^{-12} erg cm^{-2} s^{-1}. For each of the simulated spectra, the magnetic accretor model was then re-fit to the data with all the key parameters free to vary; to be conservative we treated each of the simulated spectra independently (i.e. we did not attempt to fit them together, linking parameters between them).

The results for the luminosity–temperature plane for the DISKPBB component from these simulations are shown in Fig. 5, assuming 60 ks exposures for the lower flux/higher temperature observations and 50 ks exposures for the higher flux/lower temperature observations, resulting in an overall exposure of ∼600 ks for the total set of observations. This is to be compared against the total observational investment of 1.6 Ms that went into producing the results presented in Fig. 4. Either equivalently good or superior results would be provided by *HEX-P* with a significantly smaller overall investment, and critically with no reliance on coordinated observations, demonstrating the impact that *HEX-P* would have on our understanding of the broad-band spectral evolution seen from ULXs. While the simulations presented here are primarily set up to be relevant to Holmberg IX X-1 (though they may also therefore be relevant to NGC 1313 X-1; D. J. Walton et al. 2020), there is of course significant interest in determining the evolution of the different ULX spectral components more generally (e.g. A. Gúrpide et al. 2021; A. Robba et al. 2021; F. Barra et al. 2022, 2024). A further exploration of the ULX science that would be possible with *HEX-P* is presented in M. Bachetti et al. (2023).

6 SUMMARY AND CONCLUSIONS

We have presented results from a series of five new coordinated *XMM–Newton* + *NuSTAR* X-ray observations program on the ULX Holmberg IX X-1 performed in late 2020 (bringing the total number of broad-band observations with high-energy coverage from *NuSTAR* to 11), focusing on the broad-band (∼0.3–40.0 keV) spectral evolution exhibited by this source. While Holmberg IX X-1 has previously shown evidence for remarkably stable high-energy emission above ∼10–15 keV (despite clear variations at lower energies), the first three of these new observations reveal a new 'soft' state in which the observed high-energy flux has collapsed. The last two observations show a recovery in the hard X-ray flux, which returns to its previously stable level. We consider a variety of different possible scenarios for this sudden collapse in high-energy flux, allowing for the origin of the high-energy emission to be either a Compton up-scattering corona around a non-magnetic accretor or an accretion column on to a magnetized accretor (using the known ULX pulsars as a template), as the nature of the accretor in Holmberg IX X-1 currently remains uncertain. These scenarios include obscuration by the geometrically thick super-Eddington accretion disc expected in this system (possible for both the corona and accretion column origins for the high-energy emission), a transition into the propeller regime (should the high-energy emission come from an accretion column) and the destruction and re-formation of a corona analogous to the event recently seen from the AGN 1ES 1927+654. Our current view is that the latter may be the most plausible explanation, though a definitive conclusion is challenging with the available data.

The interpretation of the high-energy emission in Holmberg IX X-1 has an important impact on the inferred behaviour of the thermal component assumed to be associated with the innermost accretion disc (the DISKPBB component in the spectral models utilized here) in the luminosity–temperature plane. Should this arise in a corona, the multi-epoch data for this component appear to trace out two distinct luminosity–temperature tracks similar to the results seen from the ULX NGC 1313 X-1: a higher flux/lower temperature track and a lower flux/higher temperature track, each of which shows a positive correlation between luminosity and temperature. Should the high-energy emission instead arise from an accretion column the behaviour is more complex, with the new soft-state observations separating themselves from the other high-flux observations that have 'normal' levels of high-energy emission. It could still be the case that two distinct luminosity–temperature tracks (similar to NGC 1313 X-1) are seen outside of this new soft state, but with only two such epochs currently available this remains highly speculative. Understanding the nature of this soft state and the luminosity–temperature behaviour of the accretion disc in Holmberg IX X-1 are closely linked, but further broad-band observations of Holmberg IX X-1 will be required to shed more light on these issues.

DATA AVAILABILITY

The raw observational data underlying this article are all publicly available from ESA's *XMM–Newton* Science Archive[6] and NASA's HEASARC archive.[7]

REFERENCES

Arnaud K. A., 1996, in Jacoby G. H., Barnes J., eds, ASP Conf. Ser. Vol. 101, Astronomical Data Analysis Software and Systems V. Astron. Soc. Pac., San Francisco, p. 17

Asai K. et al., 2013, ApJ, 773, 117

Bachetti M., 2018, Astrophysics Source Code Library, record ascl:1805.019

Bachetti M. et al., 2013, ApJ, 778, 163

Bachetti M. et al., 2014, Nature, 514, 202

Bachetti M. et al., 2020a, StingraySoftware/stingray: Version 0.2, Zenodo, Version v0.2

Bachetti M. et al., 2020b, ApJ, 891, 44

Bachetti M. et al., 2022, ApJ, 937, 125

Bachetti M. et al., 2023, Frontiers Astron. Space Sci., 10, 1289432

Barra F. et al., 2022, MNRAS, 516, 3972

Barra F., Pinto C., Middleton M., Di Salvo T., Walton D. J., Gúrpide A., Roberts T. P., 2024, A&A, 682, A94

Berghea C. T., Johnson M. C., Secrest N. J., Dudik R. P., Hennessy G. S., El-khatib A., 2020, ApJ, 896, 117

Boller T. et al., 2003, A&A, 397, 557

Brightman M. et al., 2016, ApJ, 816, 60

Brightman M. et al., 2022, ApJ, 925, 18

Burrows D. N. et al., 2005, Space Sci. Rev., 120, 165

Carpano S., Haberl F., Maitra C., Vasilopoulos G., 2018, MNRAS, 476, L45

Chashkina A., Lipunova G., Abolmasov P., Poutanen J., 2019, A&A, 626, A18

Corbel S., Fender R. P., Tzioumis A. K., Tomsick J. A., Orosz J. A., Miller J. M., Wijnands R., Kaaret P., 2002, Science, 298, 196

Corbel S., Kaaret P., Fender R. P., Tzioumis A. K., Tomsick J. A., Orosz J. A., 2005, ApJ, 632, 504

Cseh D. et al., 2014, MNRAS, 439, L1

Cseh D. et al., 2015, MNRAS, 452, 24

Cui W., 1997, ApJ, 482, L163

D'Aì A. et al., 2021, MNRAS, 507, 5567

den Herder J. W. et al., 2001, A&A, 365, L7

Doroshenko V., Santangelo A., Ducci L., 2015, A&A, 579, A22

Dudik R. P., Berghea C. T., Roberts T. P., Grisé F., Singh A., Pagano R., Winter L. M., 2016, ApJ, 831, 88

Earnshaw H. P. et al., 2019, ApJ, 881, 38

Evans P. A. et al., 2009, MNRAS, 397, 1177

Fürst F. et al., 2016, ApJ, 831, L14

Fürst F. et al., 2021, A&A, 651, A75

Gallo L. C., MacMackin C., Vasudevan R., Cackett E. M., Fabian A. C., Panessa F., 2013, MNRAS, 433, 421

Gehrels N. et al., 2004, ApJ, 611, 1005

Gladstone J. C., Roberts T. P., Done C., 2009, MNRAS, 397, 1836

Gúrpide A., Godet O., Koliopanos F., Webb N., Olive J. F., 2021, A&A, 649, A104

Harrison F. A. et al., 2013, ApJ, 770, 103

HI4PI Collaboration, 2016, A&A, 594, A116

Huppenkothen D. et al., 2019, ApJ, 881, 39

Illarionov A. F., Sunyaev R. A., 1975, A&A, 39, 185

Israel G. L. et al., 2017a, Science, 355, 817

Israel G. L. et al., 2017b, MNRAS, 466, L48

Jansen F. et al., 2001, A&A, 365, L1

Kawashima T., Ohsuga K., Mineshige S., Yoshida T., Heinzeller D., Matsumoto R., 2012, ApJ, 752, 18

King A. R., 2008, MNRAS, 385, L113

King A. R., Davies M. B., Ward M. J., Fabbiano G., Elvis M., 2001, ApJ, 552, L109

King A., Lasota J.-P., Middleton M., 2023, New Astron. Rev., 96, 101672

Koliopanos F., Vasilopoulos G., Godet O., Bachetti M., Webb N. A., Barret D., 2017, A&A, 608, A47

Kosec P., Pinto C., Fabian A. C., Walton D. J., 2018a, MNRAS, 473, 5680

Kosec P., Pinto C., Walton D. J., Fabian A. C., Bachetti M., Brightman M., Fürst F., Grefenstette B. W., 2018b, MNRAS, 479, 3978

Kosec P. et al., 2021, MNRAS, 508, 3569

Lau R. M. et al., 2019, ApJ, 878, 71

Luangtip W., Roberts T. P., Done C., 2016, MNRAS, 460, 4417

Lutovinov A. A., Tsygankov S. S., Karasev D. I., Molkov S. V., Doroshenko V., 2019, MNRAS, 485, 770

Madsen K. K. et al., 2024, Frontiers Astron. Space Sci., 11, 1357834

Masterson M. et al., 2022, ApJ, 934, 35

McClintock J. E., Remillard R. A., Rupen M. P., Torres M. A. P., Steeghs D., Levine A. M., Orosz J. A., 2009, ApJ, 698, 1398

Middleton M. J. et al., 2013, Nature, 493, 187

Middleton M., Gúrpide A., Walton D. J., 2023, MNRAS, 519, 2224

Miller J. M., Fabbiano G., Miller M. C., Fabian A. C., 2003, ApJ, 585, L37

Miller J. M., Walton D. J., King A. L., Reynolds M. T., Fabian A. C., Miller M. C., Reis R. C., 2013, ApJ, 776, L36

Mineshige S., Hirano A., Kitamoto S., Yamada T. T., Fukue J., 1994, ApJ, 426, 308

Mitsuda K. et al., 1984, PASJ, 36, 741

Mitsuda K. et al., 2007, PASJ, 59, S1

Mukherjee E. S. et al., 2015, ApJ, 808, 64

Mushtukov A. A., Suleimanov V. F., Tsygankov S. S., Ingram A., 2017, MNRAS, 467, 1202

Narayan R., Sa̧dowski A., Soria R., 2017, MNRAS, 469, 2997

Parfrey K., Tchekhovskoy A., 2017, ApJ, 851, L34

Paturel G., Theureau G., Fouqué P., Terry J. N., Musella I., Ekholm T., 2002, A&A, 383, 398

Piconcelli E., Jimenez-Bailón E., Guainazzi M., Schartel N., Rodríguez-Pascual P. M., Santos-Lleó M., 2004, MNRAS, 351, 161

Pinto C., Walton D. J., 2023, preprint (arXiv:2302.00006)

Pinto C., Middleton M. J., Fabian A. C., 2016, Nature, 533, 64

Pinto C. et al., 2017, MNRAS, 468, 2865

Pinto C. et al., 2020, MNRAS, 492, 4646

Pintore F. et al., 2025, A&A, 695, A238

Poutanen J., Lipunova G., Fabrika S., Butkevich A. G., Abolmasov P., 2007, MNRAS, 377, 1187

Rana V. et al., 2015, ApJ, 799, 121

Ransom S. M., Eikenberry S. S., Middleditch J., 2002, AJ, 124, 1788

Remillard R. A., McClintock J. E., 2006, ARA&A, 44, 49

Ricci C. et al., 2020, ApJ, 898, L1

Robba A. et al., 2021, A&A, 652, A118

Rodríguez Castillo G. A. et al., 2020, ApJ, 895, 60

Sathyaprakash R. et al., 2019, MNRAS, 488, L35

Sazonov S. Y., Lutovinov A. A., Krivonos R. A., 2014, Astron. Lett., 40, 65

Shakura N. I., Sunyaev R. A., 1973, A&A, 24, 337

Steiner J. F., Narayan R., McClintock J. E., Ebisawa K., 2009, PASP, 121, 1279

[6] https://www.cosmos.esa.int/web/xmm-newton/xsa
[7] https://heasarc.gsfc.nasa.gov/

Steiner J. F. et al., 2011, MNRAS, 416, 941
Steiner J. F., McClintock J. E., Reid M. J., 2012, ApJ, 745, L7
Stobbart A.-M., Roberts T. P., Wilms J., 2006, MNRAS, 368, 397
Strohmayer T. E., Mushotzky R. F., 2009, ApJ, 703, 1386
Strüder L. et al., 2001, A&A, 365, L18
Sutton A. D., Roberts T. P., Middleton M. J., 2013, MNRAS, 435, 1758
Tomsick J. A., Corbel S., Fender R., Miller J. M., Orosz J. A., Tzioumis T., Wijnands R., Kaaret P., 2003, ApJ, 582, 933
Tsygankov S. S., Lutovinov A. A., Doroshenko V., Mushtukov A. A., Suleimanov V., Poutanen J., 2016, A&A, 593, A16
Turner M. J. L. et al., 2001, A&A, 365, L27
Urquhart R., Soria R., 2016, MNRAS, 456, 1859
van der Klis M., 1989, in Ögelman H., van den Heuvel E. P. J., eds, Timing Neutron Stars, vol. 262 of NATO Advanced Study Institute (ASI) Series C, Kluwer Academic / Plenum Publishers, New York, p.27
Vasilopoulos G., Petropoulou M., Koliopanos F., Ray P. S., Bailyn C. B., Haberl F., Gendreau K., 2019, MNRAS, 488, 5225
Verner D. A., Ferland G. J., Korista K. T., Yakovlev D. G., 1996, ApJ, 465, 487
Walton D. J. et al., 2013a, ApJ, 779, 148
Walton D. J., Miller J. M., Harrison F. A., Fabian A. C., Roberts T. P., Middleton M. J., Reis R. C., 2013b, ApJ, 773, L9
Walton D. J. et al., 2014, ApJ, 793, 21
Walton D. J. et al., 2015a, ApJ, 799, 122
Walton D. J. et al., 2015b, ApJ, 806, 65
Walton D. J. et al., 2016a, ApJ, 826, L26
Walton D. J. et al., 2016b, ApJ, 826, 87
Walton D. J. et al., 2017a, ApJ, 839, 105
Walton D. J. et al., 2017b, ApJ, 839, 110
Walton D. J. et al., 2018a, ApJ, 857, L3
Walton D. J. et al., 2018b, MNRAS, 473, 4360
Walton D. J. et al., 2018c, ApJ, 856, 128
Walton D. J. et al., 2020, MNRAS, 494, 6012
Watarai K.-y., Fukue J., Takeuchi M., Mineshige S., 2000, PASJ, 52, 133
Wilms J., Allen A., McCray R., 2000, ApJ, 542, 914

APPENDIX A: PULSATION SEARCHES

In addition to the spectral analysis presented in the main body of the paper, we have also undertaken pulsation searches for all of the *XMM–Newton* and *NuSTAR* observations of Holmberg IX X-1 presented here, analysing the data from each epoch independently (we focus on these observatories as they have detectors with sufficient temporal resolution to detect the spin periods of $\sim$1 s or less seen in most ULX pulsars). To facilitate these searches, all photon arrival times were transferred to the solar barycenter using the DE200 solar ephemeris.

To account for the high spin up rates commonly found in PULXs, we ran an accelerated Fourier-domain search (S. M. Ransom, S. S. Eikenberry & J. Middleditch 2002), implemented in the tool HENaccelsearch included in the HENDRICS software package (M. Bachetti 2018). For *NuSTAR* observations the maximum frequency investigated was 1000 Hz, while for *XMM–Newton* observations it was between $\sim$7 and 200 Hz, depending on whether the observation was taken in full frame or small window mode. *NuSTAR* events from FPMA and FPMB were merged into a single event list for this analysis in order to improve the signal-to-noise ratio. Events outside good time intervals were rejected.

Internally, HENaccelsearch substitutes the light curve outside GTIs with the mean of the two adjacent GTIs. To overcome the loss of sensitivity of the power density spectrum (PDS) close to the borders of the spectral bins, we used 'interbinning', a way to interpolate the signal between two bins using the signal in the adjacent bins (M. van der Klis 1989). This search technique produces many false positives due to the alteration of the white noise level of the PDS, all of which need to be confirmed with independent methods. We found

$\sim$100 candidates over the whole frequency band. Most of them were at very low frequencies, clustered around specific frequencies and their harmonics which could be traced to beats of the orbital period. A few turned out to be clear artefacts (like sub-harmonics of the sampling frequency, recognizable by the step-function shape of the folded profile) and were rejected.

We then analysed the $f - \dot{f}$ parameter space around all remaining candidate frequencies with the Z_1^2 (i.e. a Rayleigh test). To perform this analysis, we used the tool HENzsearch with the 'fast' option; this optimizes the search in the $\dot{f}$ space by pre-binning the photons in phase and computing the Z_n^2 statistic using these bins instead of the individual photons, a technique referred to as the quasi-fast folding algorithm (D. Huppenkothen et al. 2019; M. Bachetti et al. 2020a).

Most of the candidates were not confirmed as significant by the Z_1^2 search, which is due to the altered statistical properties of interbinning. Several candidates at high power ($Z_1^2 \gtrsim 50$) appeared, which would normally be considered detections, but given the high number of trial frequencies and frequency derivatives spanned by the acceleration search process, the interbinning and the interpolation outside of GTIs, it is difficult to quantify exactly the number of trials involved, and in turn, evaluate their significance. Moreover, none of the candidates showed up in more than one data set, or in both of the paired, quasi-simultaneous *XMM–Newton* and *NuSTAR* observations, which makes it unlikely they represent the rotation of a neutron star. As such, we do not report any significant detection of pulsations from these observations, and adopt the position throughout the main paper that the nature of the accretor in Holmberg IX X-1 remains unknown.

APPENDIX B: FURTHER DISCUSSION OF THE NATURE OF THE SOFT STATE

As noted in Section 4.2, though these were ultimately deemed unlikely to be viable explanations, here we provide further discussion of the two remaining scenarios considered for the soft state in Holmberg IX X-1, providing our reasoning as to why we consider them unlikely.

B1 Formation of a 'scattersphere'

A possibility somewhat related to the obscuration scenario (Section 4.2.1) is that we are typically viewing Holmberg IX X-1 down the funnel formed by a super-Eddington disc/wind (as may be expected given its typically hard spectral shape; A. D. Sutton, T. P. Roberts & M. J. Middleton 2013), but that during the soft state the optical depth of the material inside the funnel itself becomes optically thick to electron scattering, with the resulting 'scattersphere' blocking our view of the inner regions (instead of the outer disc/wind). R. Narayan, A. Sa̧dowski & R. Soria (2017) suggest this can result in a significant softening of the osberved spectrum (see also T. Kawashima et al. 2012), particularly if the scattersphere lies at a large distance from the accretor where temperatures are cooler. However, this scenario would be expected to produce a significantly enhanced soft X-ray flux during the soft state relative to the other high-flux epochs. The formation of such a scattersphere may require an increase in accretion rate through the disc, but even if it can be produced by other changes in the disc structure while $\dot{m}$ remains $\sim$constant, all of the hidden high-energy flux should now be down-scattered to the temperature of the scattersphere and emerge at these energies instead. Such an enhancement in soft X-ray flux is not obviously seen though (see Table 3).

B2 Propeller transition

Should Holmberg IX X-1 be powered by a magnetized neutron star, such that the highest energy flux is associated with emission from one or more accretion columns, another interesting possibility is that the disappearance of the high-energy flux is related to a transition to the propeller regime.[8] The propeller regime corresponds to a state in which the material at the magnetosphere is not rotating fast enough to couple to the rotating magnetic field of the central object, meaning that the inflow of material through the magnetosphere is not possible (e.g. A. F. Illarionov & R. A. Sunyaev 1975). Whether a source is in the propeller regime thus depends on whether the magnetospheric radius (R_M) is inside or outside the 'co-rotation' radius (R_{co}; the radius at which the orbital motion in the disc matches the rotation period of the central object). If $R_M < R_{co}$ then the material is rotating fast enough and accretion can proceed down to the neutron star surface, while if $R_M > R_{co}$ then the material is not rotating fast enough and accretion through the magnetosphere is halted.

Since R_M is generally expected to depend on the accretion rate (e.g. W. Cui 1997), it is possible for sources to transition to and from the propeller regime. Typically, transitions to the propeller regime are expected to be associated with a catastrophic drop in X-ray flux, corresponding to the sudden cessation of accretion through the magnetosphere (e.g. W. Cui 1997; K. Asai et al. 2013; S. S. Tsygankov et al. 2016; A. A. Lutovinov et al. 2019). However, if there is substantial X-ray emission from a super-Eddington accretion disc outside of the magnetosphere then it may be possible to sustain a high overall observed flux, with the catastrophic drop limited to the energies at which the emission from within R_M dominates. Indeed, phase-resolved spectral decomposition of the known ULX pulsars implies there is a significant contribution from non-pulsed thermal emission in addition to the pulsed component associated with the accretion column (D. J. Walton et al. 2018b, c). Furthermore, in some of the ULX pulsars the pulsations are seen to come and go without large changes in soft X-ray flux (e.g. G. L. Israel et al. 2017a), which could potentially be due to the accretion column shutting off after a propeller transition (resulting in a lack of pulsations) while the X-ray-emitting super-Eddington disc outside of R_M remains (see also M. Middleton, A. Gúrpide & D. J. Walton 2023).

A significant issue here, however, is that propeller transitions are usually expected to be seen at low-accretion rates as they are generally thought to be driven by changes in accretion rate moving R_M outside R_{co}, and the collapse of the high-energy flux in Holmberg IX X-1 is actually seen during relatively bright observations. In order for this to be the case, we would require that the observations corresponding to the lower flux/higher temperature group in Fig. 4 actually have higher accretion rates than the rest of the broad-band observations. In turn, this would require that the complex luminosity–temperature behaviour is caused by something along the lines of the scattering wind scenario described above (the sort of evolution shown in the right-hand panel from fig. 7 in D. J. Walton et al. 2020). However, we note again that the similarity of the highest energy flux between the lower flux/higher temperature observations and the 'normal' higher flux/lower temperature observations is very difficult to explain in this scenario, as the emission from the accretion columns must come from even smaller scales than the inner disc, and so any screen that results in a suppression of the observed flux from the inner disc should realistically also result in a suppression of the observed flux from the accretion columns as well.

Alternatively, given that what ultimately needs to occur for a propeller transition is a switch from $R_M < R_{co}$ to $R_M > R_{co}$, a propeller transition could potentially be driven by a change in R_{co} instead of R_M (M. Middleton et al. 2023). Indeed, in the model of super-Eddington accretion on to a magnetized neutron star constructed by A. Chashkina et al. (2019), over a limited range of accretion rates R_M actually becomes essentially independent of the accretion rate,[9] and so any propeller transitions that occur in this regime may have to invoke changes in R_{co}. Having propeller transitions can be driven by changes in R_{co} would remove the expectation that such transitions must be seen at lower luminosities.

Although the spin-up rates in ULX pulsars can be large (e.g. M. Bachetti et al. 2014; S. Carpano et al. 2018), potentially resulting in appreciable changes in R_{co} on observable time-scales, even in these systems the spin periods (P) do not change by large factors over the ∼decade time-scales they have been observed (M. Bachetti et al. 2020b, 2022; F. Fürst et al. 2021).[10] Furthermore, R_{co} has a moderately shallow dependence on P (it should scale as $R_{co} \propto P^{2/3}$). Invoking a propeller transition driven by changes in P would place a strong requirement that the source was already extremely close to spin equilibrium (i.e. $R_{co} \simeq R_M$). It is also unclear whether accretion at a relatively steady rate could genuinely spin-up the neutron star to the point where it enters the propeller regime. As the neutron star approaches spin equilibrium the spin-up rate should taper off (as the disc can impart less and less angular momentum), meaning that R_{co} may only be able to asymptote towards R_M, but not cross it, if only P is changing. It may be easier, instead, to invoke changes in the orbital frequencies within the disc, e.g. due to changing viscosity, as a mechanism for inducing a propeller transition by changing R_{co}. However, the similar soft X-ray fluxes ($\lesssim 2\,$keV) seen in the soft state epochs to the other high-flux epochs would suggest there are not large changes in accretion rate through the disc, so this would likely also require $R_{co} \simeq R_M$. Given all of this, it is not clear whether the propeller regime really offers a plausible scenario for the soft state observations in Holmberg IX X-1; this might only be possible under very specific circumstances.

---

[8]3D general-relativistic magnetohydrodynamic simulations have shown that even when a source is in the propeller regime, occasionally it is still possible for small amounts of material to penetrate down to the neutron star owing to the turbulent nature of the accreting material outside of the magnetosphere, even though significant, continuous accretion rates are prevented (K. Parfrey & A. Tchekhovskoy 2017). As such, this small amount of high-energy flux may not be an issue for this possibility.

[9]This occurs when the disc is dominated by radiation pressure, which sits in between the regimes in which the disc is dominated by gas pressure (lower accretion rates) and in which advection starts to play a major role (the highest accretion rates), but the quantitative range of accretion rates over which R_M remains constant depends on the magnetic field of the neutron star.

[10]NGC 300 ULX1 is a notable exception, which does change its spin period significantly on these time-scales (G. Vasilopoulos et al. 2019).

This paper has been typeset from a TEX/LATEX file prepared by the author.